SUPPLEMENTARY MATERIAL

ABC ATPase signature helices in Rad50 link nucleotide state to Mre11 interface for DNA double-strand break repair

Gareth J. Williams, R. Scott Williams, Jessica S. Williams, Gabriel Moncalian, Andy Arvai, Oliver Limbo, Grant Guenther, Soumita SilDas, Michal Hammel, Paul Russell, and John A. Tainer

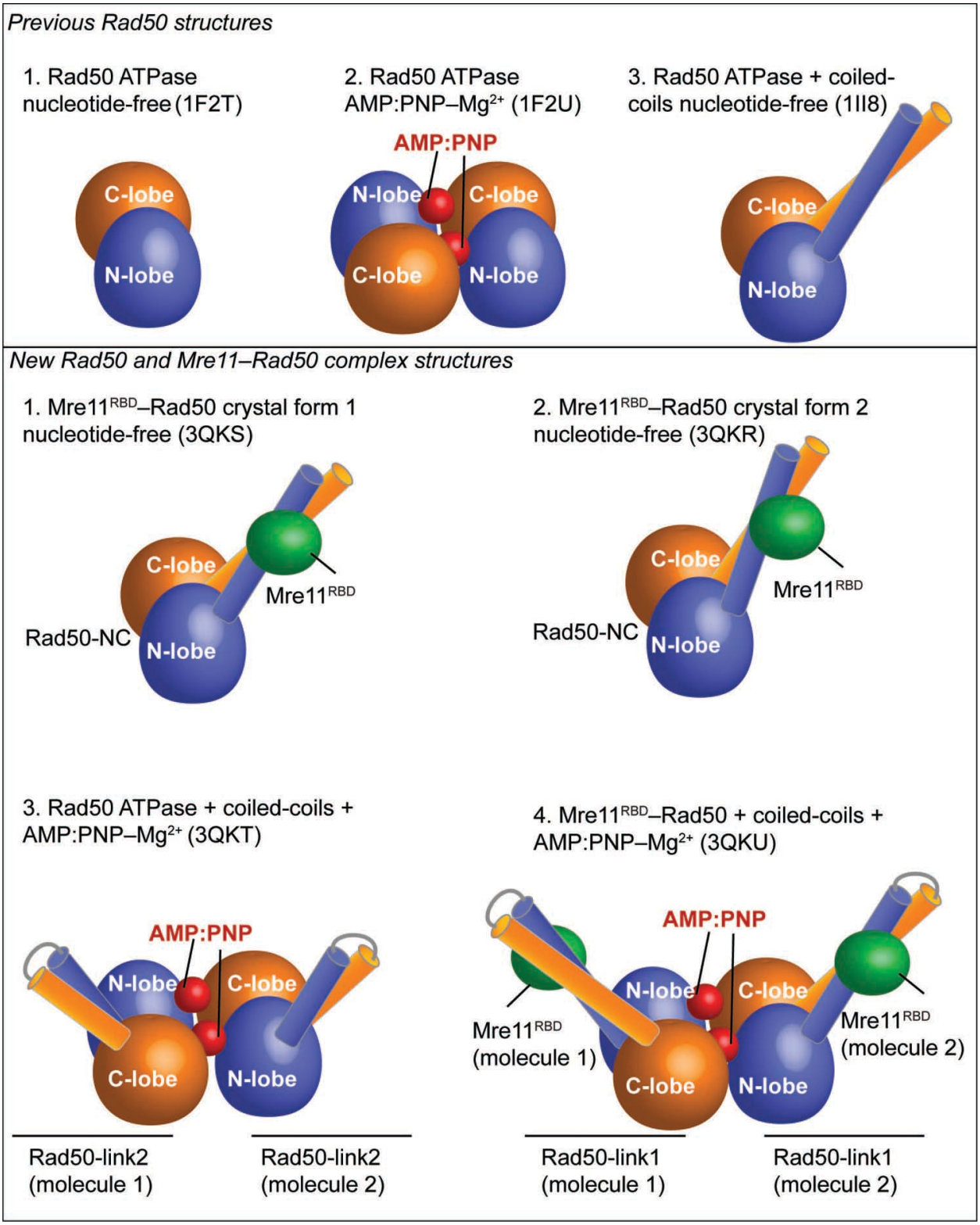

Supplementary Fig. 1. Schematic of previously available and novel Rad50 structures.

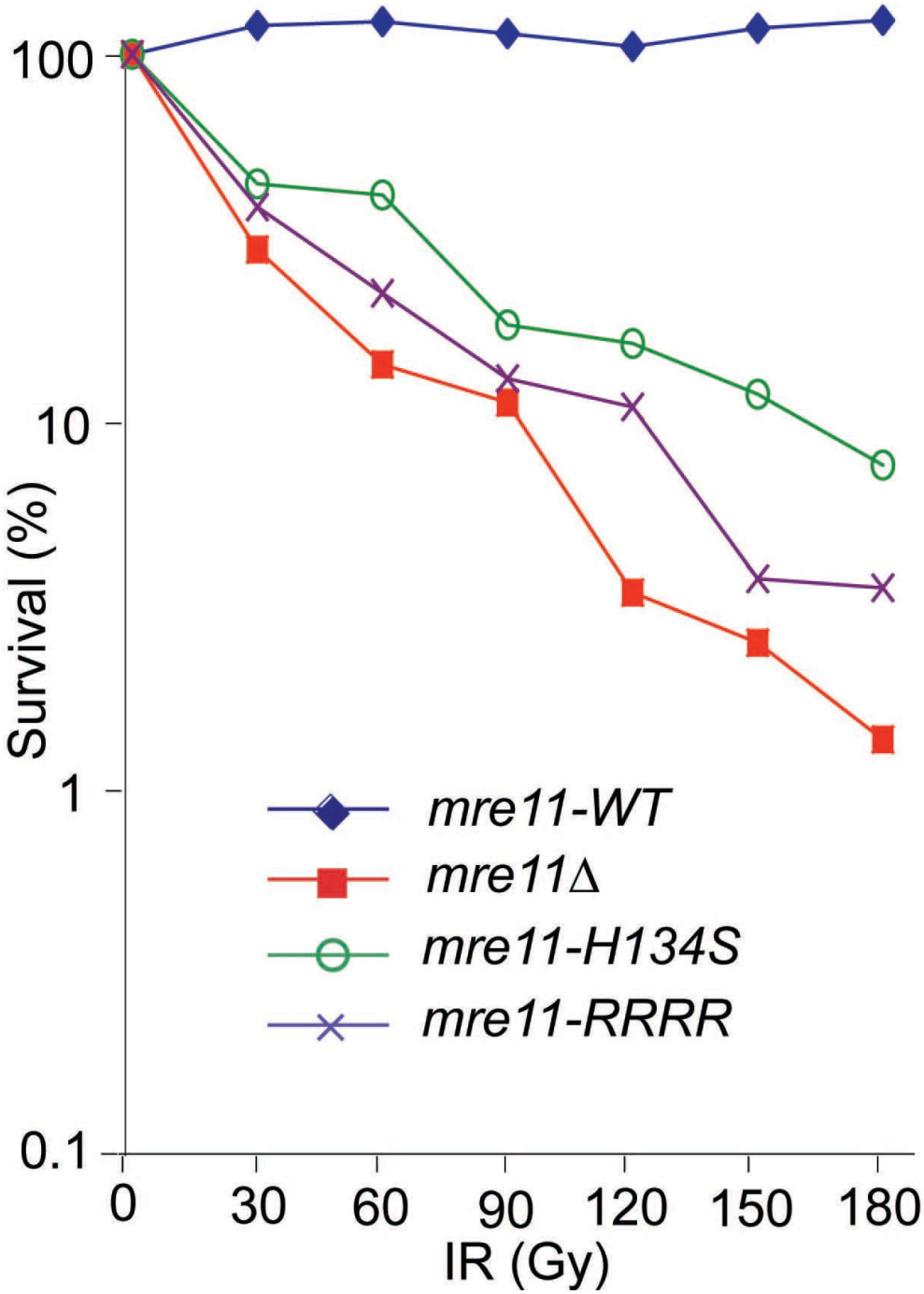

Supplementary Figure 2. Survival plot showing Mre11 RBD variants are IR sensitive. This plot is representative of two independent experiments (Also see Fig. 3c).

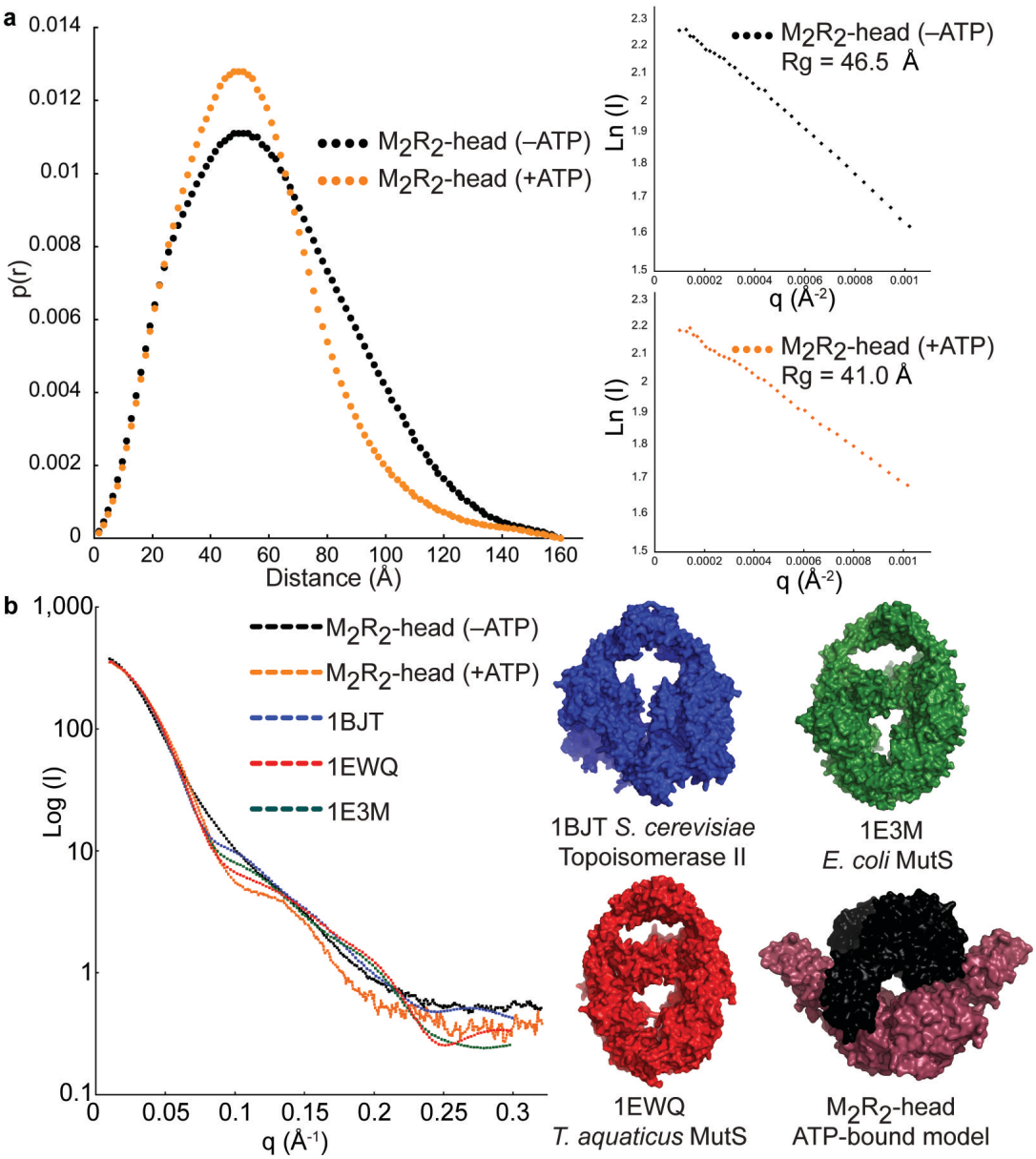

Supplementary Figure 3. SAXS data of the M_2R_2-head support a toroidal architecture. (**a**) Pair distribution plots show compaction of the M_2R_2-head architecture in the presence of ATP (left). Guinier analysis (right) show samples are free from aggregates and that ATP-binding induces an Rg change of 4.5 Å. (**b**) Structures present in the PDB with the most similar architecture to the M_2R_2-head are all toroidal. Scattering curves (left) compare theoretical curves calculated from the structures identified by DARA searches (right; shown as surface representations with PDB code and common name) that most closely match the experimental scattering from the M_2R_2-head. As a comparison of architecture, our ATP-bound M_2R_2-head model is shown.

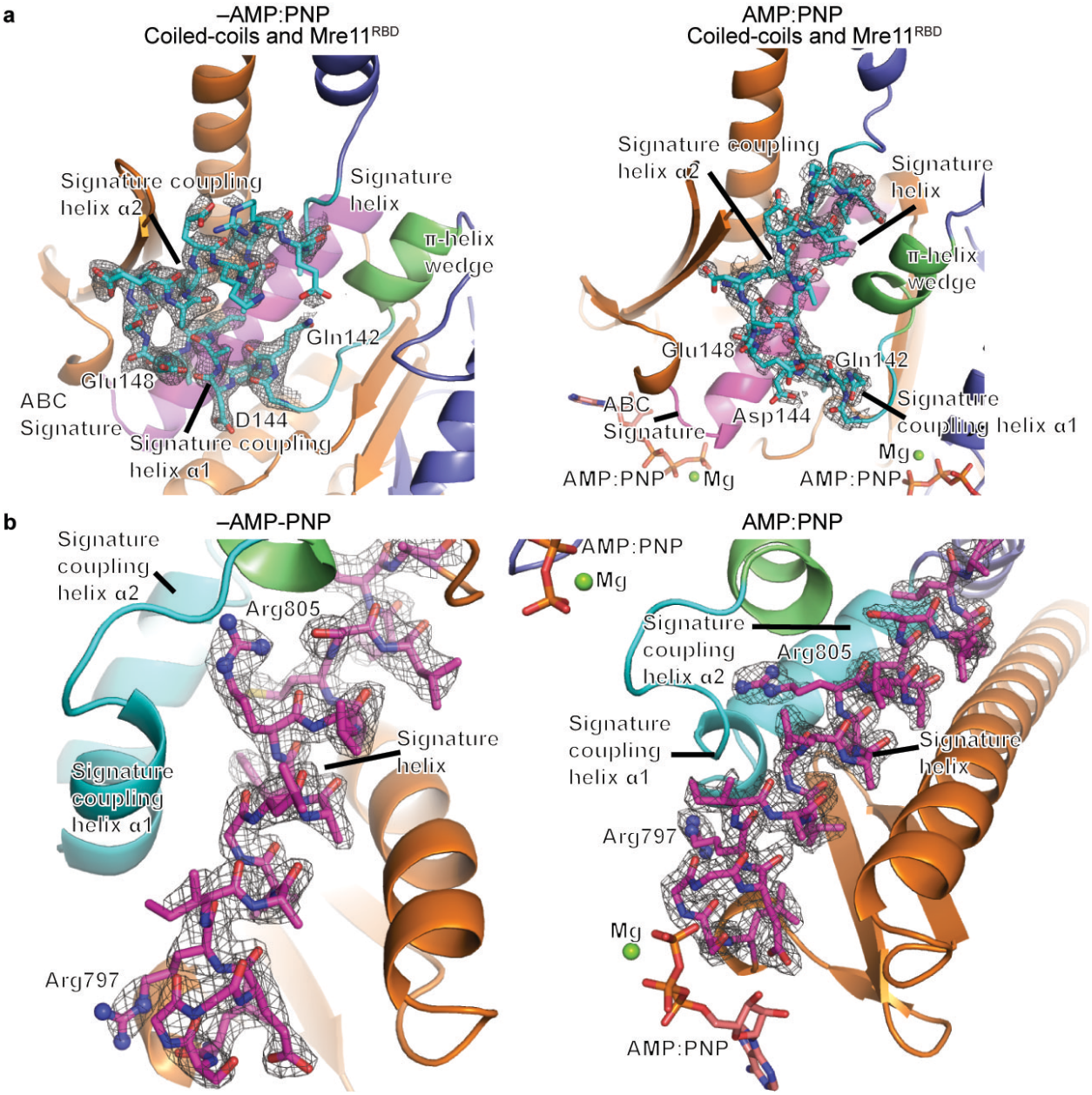

Supplementary Figure 4. Conformational changes of Rad50 signature coupling helices and signature helix. Experimental density, simulated annealing 2FoFc omit map shown (gray), supports the key conformations observed in nucleotide-free and -bound states (also see main text Fig. 5). (**a**) Density for the signature coupling helices shows that it switches to an open conformation upon nucleotide binding. (**b**) Density for the signature helix showing that the Arg797 and Arg805 switches rearrange following nucleotide binding. Colored as in Fig. 5.

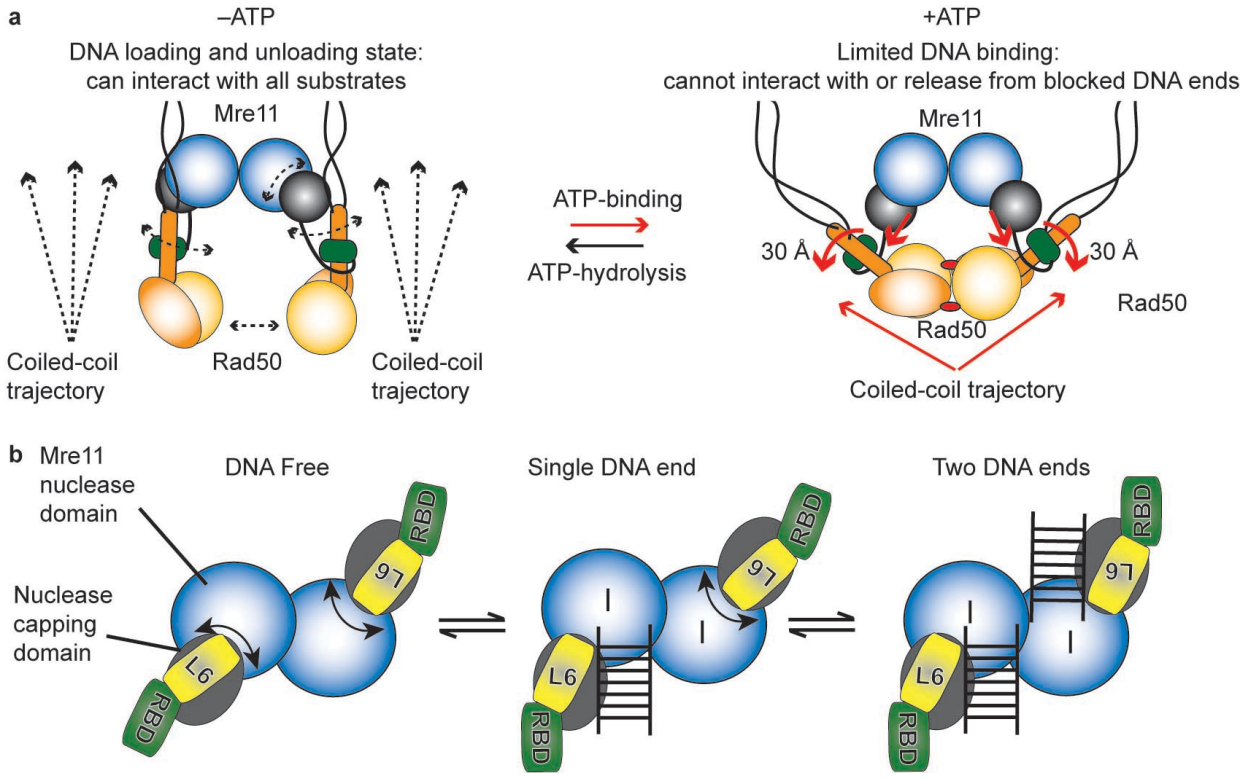

Supplementary Figure 5. Mre11–Rad50 conformational controls. (**a**) Model of how ATP-driven Rad50 conformational changes may influence Mre11. In the ATP-free state (–ATP) significant conformational flexibility exists (shown by dashed arrows) in the Mre11–Rad50 complex as observed by our crystal and SAXS solution structures. In the ATP-bound state (+ATP) the Mre11–Rad50 complex closes, resulting in key domains becoming rigid and or repositioned (shown by solid red arrows). These movements include Rad50 subdomain rotations, which must pull on Mre11 nuclease domains through repositioning the coiled-coil and attached Mre11 RBD ~30 Å. We hypothesize that in the ATP-free, more conformationally open and flexible state, Mre11 can interact with and disassemble from any of its potential substrates. Upon ATP-binding, the closure of the M_2R_2-head would prevent loading onto substrates with blocked ends. (**b**) Proposed role for conformational change and symmetry transitions associated with Mre11 DNA binding. Movement of Mre11 capping domain signals Mre11 DNA binding state to the proximal Mre11 RBD and attached Rad50 ATPase domain. Undefined ATP-dependent Rad50 control of Mre11 nuclease capping domain likely influences Mre11 endonuclease and exonuclease activities.

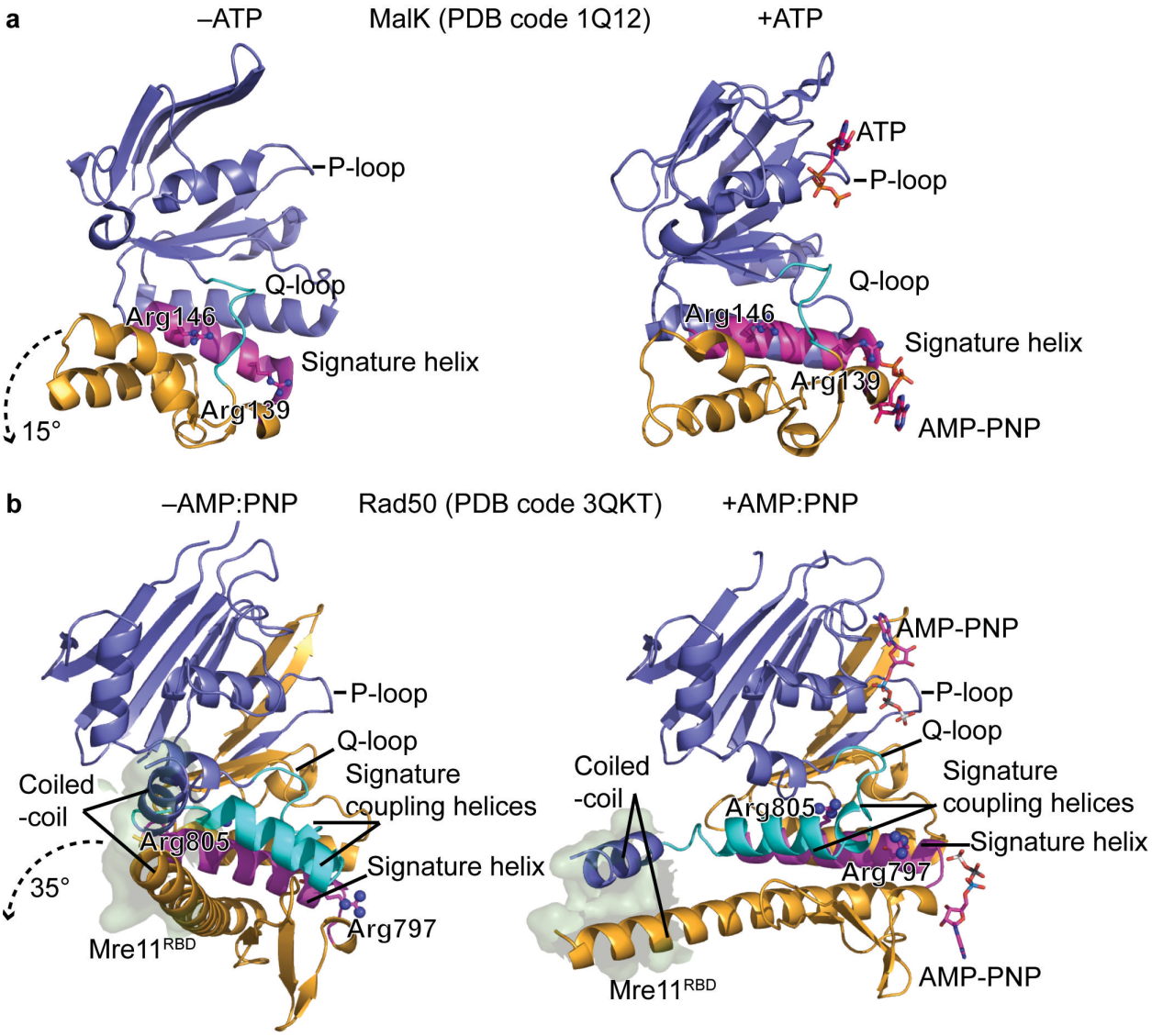

Supplementary Figure 6. Comparison of conformational changes upon nucleotide binding in ABC-ATPases. (**a**) "Membrane view" of the MalK ABC-ATPase subunit of the maltose transporter. The α–helical subdomain (orange) rotates ~15° with respect to the RecA-like subdomain (blue). The Q-loop (cyan), signature helix (magenta) and equivalent residues to Rad50 basic-switches are highlighted. (**b**) Equivalent "Mre11-view" of Rad50 shows that the C-lobe (orange), which is equivalent to the ABC transporter α–helical subdomain, rotates ~35° with respect to the RecA-subdomain. Coloring of motifs is as in main text Fig. 5.

Supplementary Movies 1, 2 and 3. Nucleotide-induced Rad50 conformational changes**.** Rad50 structures with coiled-coil regions in the absence (start position) and presence (end position) of nucleotide were superimposed and movies generated by morphing between states in PyMOL (DeLano Scientific LLC, Palo Alto, CA, U.S.A. http://www.pymol.org). Supplementary Movie 1 shows the N-lobe rotation with respect to the C-lobe. Supplementary Movie 2 shows the C-lobe rotation with respect to the N-lobe. Supplementary Movie 3 shows the C-lobe rotation with respect to the N-lobe from the side. The extended signature motif (magenta) and signature coupling helices (cyan) are highlighted. Residues in the text are shown as sticks with the extended signature motif basic-switch residues (Arg797 and Arg805) highlighted by representation of side chain nitrogens as spheres. To relate the movements to nucleotide binding AMP:PNP is shown as sticks, although it is only observed in the structure of the nucleotide bound form. To relate the movements to bound Mre11 RBD, residues on the Rad50 coiled-coils involves in the $Mre11^{RBD}$–Rad50 interface are shown in a green transparent surface representation. For clarity only one Rad50 molecule is shown, although in structures in the presence of nucleotide dimerization occurs with AMP:PNP sandwiched between ABC-ATPase domains.

Supplementary Table 1. *S. pombe* strains used in this study

Name	Strain	Genotype	Source
WT (untagged)	PR110	*h⁺ ura4-D18 leu1-32*	Lab stock
mre11Δ	YY4321	*h⁺ ura4-D18 leu1-32 mre11::KanMx*	Lab stock[1]
exo1Δ	OL4175	*h⁻ ura4-D18 leu1-32 exo1::ura4⁺*	Lab stock[2]
exo1Δ pku80Δ	OL4176	*h⁻ ura4-D18 leu1-32 exo1::ura4⁺ Pku80::HphMx*	Lab stock[2]
pku80Δ	SC4083	*h⁻ ura4-D18 leu1-32 pku80::HphMx*	Lab stock[2]
mre11-RRRR	JW4713	*h⁺ ura4-D18 leu1-32 mre11-CL454RR-CV479RR-13Myc:KanMx*	This study
mre11-CL454RR	JW4711	*h⁺ ura4-D18 leu1-32 mre11-CL454RR-13Myc:KanMx*	This study
mre11-CV479RR	JW4712	*h⁺ ura4-D18 leu1-32 mre11-CV479RR-13Myc:KanMx*	This study
mre11-RRRR exo1Δ	JW4809	*h⁺ ura4-D18 leu1-32 mre11-CL454RR-CV479RR-13Myc:KanMx 0 exo1::ura4⁺*	This study
mre11-RRRR pku80Δ	JW4810	*h⁻ ura4-D18 leu1-32 mre11-CL454RR-CV479RR-13Myc:KanMx pku80::HphMx*	This study
mre11-RRRR exo1Δ pku80Δ	JW4811	*h⁻ ura4-D18 leu1-32 mre11-CL454RR-CV479RR-13Myc:KanMx exo1::ura4⁺ pku80::HphMx*	This study
mre11⁺	JW4166	*h⁺ ura4-D18 leu1-32 mre11-13Myc:KanMx*	Lab stock[1]
mre11-H134S	JW4171	*h⁻ ura4-D18 leu1-32 mre11-H134S-13Myc:KanMx*	Lab stock[1]
WT (untagged)	PR109	*h⁻ leu1-32 ura4-D18*	Lab stock
rad50Δ	OL4967	*h⁻ leu1-32 ura4-D18 rad50::kanMX6*	This study
TAP-rad50	OL4968	*h⁻ leu1-32 ura4-D18 TAP-rad50:kanMX6*	This study
TAP-rad50-K1187A	OL4969	*h⁻ leu1-32 ura4-D18 TAP-rad50-K1187A:kanMX6*	This study
TAP-rad50-K1187E	OL4982	*h⁻ leu1-32 ura4-D18 TAP-rad50-K1187E:kanMX6*	This study
TAP-rad50-R1195A	OL4983	*h⁻ leu1-32 ura4-D18 TAP-rad50-R1195A:kanMX6*	This study
TAP-rad50-R1195E	OL4970	*h⁻ leu1-32 ura4-D18 TAP-rad50-R1195E:kanMX6*	This study

SUPPLEMENTARY METHODS

X-ray diffraction data collection, phasing and refinement. Single crystal X-ray data was collected at the Advanced Light Source (Lawrence Berkeley National Laboratory) on SIBYLS beamline 12.3.1. X-ray data reduction and scaling was performed with the HKL2000 suite[3].

Phases for structures solved in this study were obtained with molecular replacement using *P. furiosus* Rad50 models from the protein databank (PDB: 1FT2) in MOLREP[4]. For the $Mre11^{RBD}$–Rad50 crystal form 1 and crystal form 2 structures one molecule in the asymmetric unit was found. For the Rad50–link1–AMP:PNP structure four Rad50 protomers, assembled as two dimers that sandwich four AMP:PNP molecules, were found. For $Mre11^{RBD}$–Rad50–link2–AMP:PNP two Rad50 protomers were identified. Manual fitting in O (v10.0)[5] and Coot[6] produced models that were refined in REFMAC[7,8] or PHENIX[9] to resolutions and with the data statistics detailed in main text Table 1. Late stages of the refinement utilized TLS group anisotropic B-factor refinement. Structural figures were produced in PyMOL.

SAXS data processing and analysis using MD and MES. In our rigid body modeling strategy BILBOMD, molecular dynamic (MD) simulations were used to explore conformational space adopted by M_2R_2-head in the absence (–ATP) and presence (+ATP) of ATP. Crystal structures of Mre11 nuclease (PDB code 3DSC with DNA chains removed) with our new Rad50 structures were used to construct the initial atomic models for –ATP (using $Mre11^{RBD}$–Rad50 crystal form 1) and +ATP (using $Mre11^{RBD}$–Rad50–link2–AMP:PNP–Mg^{2+}) data. The initial models were constructed by connecting Mre11 residues 333 and 348, which are present in the crystal structures, with a 15 residue linker. These atomic models were used as templates for rigid body modeling using BILBOMD, as described[10]. For each registered conformation, the theoretical SAXS profile and the corresponding fit to the experimental data were calculated using the program FoXS[11]. The flexibility of the M_2R_2-head complex in the absence and presence of ATP was represented by an ensemble containing 3 different conformations (see main text Fig. 4a). The scattering from such an ensemble is readily computed by

averaging the individual scattering patterns from the conformers. To select an appropriate minimal ensemble from a pool of ~10,000 MD-generated conformations, mminimal ensemble search (MES) was employed[10]. The scattering curves from all the structures in the MD–pool were first pre-computed and the subsequent genetic algorithm-selection operators were performed using these patterns and not the structures. The final models were calculated to best fit the experimental curve $I(q)_{experiment}$ minimizing the discrepancy χ^2 between the experimental and calculated multi-conformational profile. The multicomponent scattering $I(q)$ from such a minimal ensemble was computed by averaging the individual scattering profiles from conformers: $I(q) = 1 / N\ (I_1(q) + I_2(q) + \ldots + I_N(q))$ where $I_{1,2,3\ldots N}(q)$ were the scattering profiles from the single oligomers and the momentum transfer. A similar approach was used to find an ensemble of M_2R_2-head models in the presence of ATP. In this case, due to the expected mixture of ATP bound and free states, we used MES on the models found that fit the –ATP data with ATP-bound models.

SUPPLEMENTARY REFERENCES

1. Williams, R.S. *et al*. Mre11 dimers coordinate DNA end bridging and nuclease processing in double-strand-break repair. *Cell* **135**, 97-109 (2008).

2. Limbo, O. *et al*. Ctp1 is a cell-cycle-regulated protein that functions with Mre11 complex to control double-strand break repair by homologous recombination. *Mol. Cell* **28**, 134-46 (2007).

3. Otwinowski, Z. & Minor, W. Processing of X-ray diffraction data collected in oscillation mode. *Methods Enzymol.* 276, 307-326 (1997).

4. Vagin, A. & Teplyakov, A. Molecular replacement with MOLREP. *Acta Cryst.* **D66**, 22-5 (2010).

5. Jones, T.A., Zou, J.Y., Cowan, S.W. & Kjeldgaard, M. Improved methods for building protein models in electron density maps and the location of errors in these models. *Acta Cryst.* **A47**, 110-9 (1991).

6. Emsley, P., Lohkamp, B., Scott, W.G. & Cowtan, K. Features and development of Coot. *Acta Cryst.* **D66**, 486-501.

7. Murshudov, G.N., Vagin, A.A. & Dodson, E.J. Refinement of macromolecular structures by the maximum-likelihood method. *Acta Cryst.* **D53**, 240-55 (1997).

8. Winn, M.D., Isupov, M.N. & Murshudov, G.N. Use of TLS parameters to model anisotropic displacements in macromolecular refinement. *Acta Cryst.* **D57**, 122-33 (2001).

9. Adams, P.D. *et al*. PHENIX: a comprehensive Python-based system for macromolecular structure solution. *Acta Cryst.* **D66**, 213-21 (2010).

10. Pelikan, M., Hura, G.L. & Hammel, M. Structure and flexibility within proteins as identified through small angle X-ray scattering. *Gen. Physiol. Biophys.* **28**, 174-89 (2009).

11. Schneidman-Duhovny, D., Hammel, M. & Sali, A. FoXS: a web server for rapid computation and fitting of SAXS profiles. *Nucleic Acids Res.* **38**, W540-4 (2010).